Energy Technology
Generation, Conversion, Storage, Distribution

RESEARCH ARTICLE OPEN ACCESS

A Scale-Up Study on the Continuous Production of Battery Slurry in Twin-Screw Extruders Based on Flow Behavior and Material Dispersion

Juan Fernando Meza Gonzalez[1] | Annika Völp[2] | Hermann Nirschl[1] | Frank Rhein[1]

[1]Institute of Mechanical Process Engineering and Mechanics, Karlsruhe Institute of Technology (KIT), Karlsruhe, Germany | [2]Thermo Fisher Scientific, Karlsruhe, Germany

Correspondence: Frank Rhein (frank.rhein@kit.edu)

Received: 28 August 2025 | **Revised:** 9 December 2025 | **Accepted:** 6 February 2026

Keywords: continuous mixing | Li-ion battery | process scale-up | process simulation | twin-screw extruder

ABSTRACT

Driven by the increasing demand for high-performance batteries, this study addresses the need for efficient and scalable mixing processes in battery manufacturing, focusing on continuous mixing in twin-screw extruders. While extruders can operate at different production rates, process limitations require a scale-up to larger extruder sizes to further increase production capacity. This work compares the quality of anode slurries produced under equivalent process conditions on four different scales of twin-screw extruders. It was shown that the transfer from laboratory to pilot and production scale, while maintaining consistent product quality, i.e. dispersion of the conductive additive, is feasible. Flow simulations were used to quantify the material strain in each process setup, thereby facilitating the identification of relevant scale-up criteria and even allowing for process transfer to similar but not geometrically equivalent screw geometries. Additionally, the influences of different process parameters such as screw speed and mass flow rate on the dispersion quality were quantified and compared between scales. In short, processing with a specific feed load smaller than 0.01 was shown to provide better dispersion and electrode quality across scales.

1 | Introduction

The continuous growth in demand for local energy storage has led to an increase in the production and usage of batteries. Advances in materials and production technologies make it possible to meet these growing requirements. Lithium-ion batteries (LIB) are essential in this regard because they offer high energy density and stability [1]. However, their further development and adaptation to specific applications is still limited by some key challenges, including material degradation and maintaining consistent power output over time. In addition, LIB cell production is highly sensitive to quality fluctuations, which also affect the integrity and performance of the cells [1].

The mixing process in battery manufacturing is a crucial step as it directly affects downstream processes and therefore the efficiency of the production lines. It is responsible for ensuring the proper dispersion of battery components, thereby having a significant impact on internal particle distribution within the electrodes and consequently on microstructure. Accordingly, the mixing step greatly affects the stability and behavior of battery electrodes [1, 2].

While batch mixing is a widely used method in electrode production, continuous mixing in extruders has been gaining interest in the last years [1–3]. A continuous battery slurry production approach provides a steady supply of high-quality electrode slurry for battery manufacturing. This approach allows manufacturers to significantly improve the efficiency, consistency, and scalability of the production process [1, 3]. Twin-screw eExtruders (TSE) are often used in the battery production lines as a high intensity continuous mixing device for slurry preparation [1]. It consists of two co-rotating or counter-rotating screws to convey, mix,

and transform materials through controlled shear, heat, and pressure. They offer flexibility for changing production rates and adaptation to different product requirements. This is of great interest, since scaling the production is a necessary response to increasing demand for batteries. However, it has to be ensured that slurry quality is maintained after scale-up, which usually involves an extensive analysis of various process conditions.

A higher production capacity can usually be achieved when using extruders by simply increasing the feeding rate. However, this is limited by the transport capability of the screw and the process parameters. Additionally, uncontrolled changes to these parameters may result in a loss of quality. Therefore, it is sometimes necessary to transfer the process to a larger production equipment. This is a challenging task since a change in equipment and scale will also affect process conditions and therefore product quality [2]. Usually, scaling up a process goes either from a laboratory scale into pilot- or production scale. For this reason, extruder manufacturers often employ the same geometric ratios to facilitate scale-up. However, depending on the application, scale-up factors have to be defined to maintain the quality of the product. The scale-up of continuous production in extruders has been addressed by various authors [4–9]: Patil et al. [4]. recently summarized different scale-up strategies, challenges, and models used for Hot-Melt-Extrusion (HME). Similarly, Kohlgrueber et al. [9]. provide a detailed description of scaling rules for a given target product characteristics, discussing the importance of similar flow conditions. Wesholowski et al. [5]. discuss the impact of flow rate, heat transport and energy input specially on the residence time distribution (RTD) for HME as scale-up parameter on three TSEs with different screw sizes. RTD provided a suitable technique to experimentally assess the scaling accuracy in these types of applications.

A numerical simulation of the process provides an alternative method to facilitate the scale-up task. Matic et al. [6]. applied and discussed this approach for HME applications. The study introduced a screw modeling based on the simulation of individual elements using the Smoothed Particle Hydrodynamics (SPH) method.The results aimed to reproduce a comparable thermo-mechanical load on two different extruder scales, which showed a high degree of agreement between the simulation and experimental results. Yet, the authors argue that more work is needed to fully validate the accuracy of the methodology. Additional computer-based screw modeling can also be pursued using commercially available extruder modeling tools such as SIGMA, LUDOVIC, and TSEM, as discussed by Nastaj and Wilczynski [7]. Here, the authors also address the importance of further improving the models using simulation-based optimization and the difficulty for transferring the approaches into different applications.

Concerning dispersion applications in extruders, there are few recent studies addressing this task specifically in the field of battery slurries. For instance, the importance of the shear rate and residence time on dispersion has been assessed experimentally, as discussed by Dryer et al. [10]. The study investigated volumetric scaling for dispersive mixing applications in TSE, showing the importance of maintaining the same degree of filling in the screw sections. There are also physical-mathematical approaches available, such as those described by Potente et al. [11], which predict agglomerate breakage based on shear stress and are applicable to dispersion processes in extruders. Nevertheless, depending on the materials and target scale parameters, this task is generally difficult and requires a lot of expertise and experimental validations [4]. Agur [8] showed the relevance of the specify energy consumption (SEC) as a key scale-up parameter, for extrusion processes aiming for high dispersion efficiency. The study discusses the effects of different processing conditions on changes in melt temperature, residence time, and carbon black concentration at the die during the compounding process. It also highlights the ability of extruders to reduce quality fluctuations due to feed rate oscillation. While different scale-up approaches have been developed for different extrusion applications, models that address the transfer of battery slurry specific parameters have not yet been well described.

One of the main aspects to consider when producing battery slurries is the material dispersion [2, 12–14]. Recently, Weber et al. [13] addressed the critical role of mixing intensity on the dispersion of the conductive additive in cathodes produced by extrusion. The study shows that there is an optimal range of dispersion where the properties of the electrodes are enhanced. The effect of process setup on the dispersion efficiency of conductive material such as carbon black in extruders has also been discussed in our previous work [14]. Here, simulations were compared with experiments to describe how screw configuration and process conditions affect the mechanical stress exerted by the extruder and thus inducing different dispersion states in the slurries. Simulation-based optimization coupled with experimental evaluations helps to understand different process conditions that are difficult to analyze experimentally. By simulating different extrusion setups, it is possible to identify optimal process operating conditions to maximize productivity.

The present work aims to identify proper scale-up criteria to ensure product integrity on different extruder scales. Based on our previous work [14], we transfer the findings to larger extruders scales and evaluate the effects of the screw size on the local material stress as a potential scaling factor for dispersion applications. Initially, the production of battery anode slurries on three different geometric equivalent extruder scales has been analyzed both experimentally and with simulations. Additionally, a nongeometric equivalent (alternative) extruder was implemented to step into scaling criteria for changing geometries. Product quality such as changes in particle size distribution, viscosity and electrode electrical conductivity were measured to ensure quality integrity.

2 | Methods

2.1 | Scaling Approach

There are several approaches for scaling up production in twin-screw extruders, depending on the application and the target characteristics to preserve. Some of these are for example based on thermal similarity, such as the adiabatic process and the heat transfer. Others aim instead to maintain the same flow conditions or material residence time in the extruder [4]. An overview of some of this approches can be found in Table 1.

In addition, proper scaling up usually involves a series of rules to ensure similar process conditions between scales, which may include geometric similarity, the same shear rate conditions, or the same specific feed load (SFL) [9]. The latter refers to the volumetric approach and is key to ensure a similar flow in the device. It describes the relationship between the flow rate $\dot{V}$, the screw speed n, and the screw diameter D_s, as given by $\mathrm{SFL} = \dot{V}/n\,D_s^3$ [15]. Accordingly, when aiming to scale

TABLE 1 | Overview of standard scaling-up approaches used in the HME, as described by Patil et al. [4].

Target	Equation
Adiabatic	$\dot{V}_t = \dot{V}_0 \cdot \left(\frac{D_{s,t}}{D_{s,0}}\right)^3$
Volumetric	$\dot{V}_t = \dot{V}_0 \cdot \left(\frac{D_{s,t}}{D_{s,0}}\right)^3 \cdot \frac{n_t}{n_0}$
Heat transfer	$\dot{V}_t = \dot{V}_0 \cdot \left(\frac{D_{s,t}}{D_{s,0}}\right)^2 \cdot \frac{n_t}{n_0}$
Shear rate	$\dot{\gamma} = \frac{\pi n D_s}{h}$
Spec. mech. energy	$\varepsilon = \frac{M n}{\dot{m}}$

t: target scale.
0: initial scale.

production rates, Equation (1) can be used for a constant SFL between the scales, in the form of

$$\begin{aligned} \mathrm{SFL}_t &= \mathrm{SFL}_0 \\ \dot{V}_t &= \dot{V}_0 \frac{D_{s,t}^3}{D_{s,0}^3} \frac{n_t}{n_0} \end{aligned} \tag{1}$$

Here, $\dot{V}_t$ describes a target flow rate as a function of the initial flow rate $\dot{V}_0$, taking into account both the target and initial screw diameters $D_{s,t}$ and $D_{s,0}$, respectively, as well as the ratio of the screw speed before n_0 and after n_t scaling [4]. According to this approach, in order to scale the production from the reference laboratory extruder (TSE-11) to larger scales such as the TSE-16, TSE-18, and the TSE-24, the flow rate should be increased by factor 2.98, 4.68 and 10.73 respectively, assuming a constant screw speed.

Aside from an equivalent flow condition, another parameter to consider, especially for dispersion applications such as the battery mixing step, is the degree of dispersion. The dispersion process strongly depends on the resulting shear rates and the mechanical stress in the extruder, which are again susceptible to changes in the flow conditions [14]. In this case, the specific mechanical energy consumption ε, the shear rate $\dot{\gamma}$ or the stress are promising factors to consider as additional scale-up criteria [4, 10].

Typically, the highest mechanical stress exerted by the machine occurs in the gap between the screw and the extruder barrel. The shear rate

$$\dot{\gamma} = \frac{\pi D_s n}{h} \tag{2}$$

is given as a function of the screw speed n, the screw size D_s and the gap size h between the extruder barrel and the screw, where the numerator represents the circumferential speed of the screws [15]. However, in order to truly maintain a comparable stress, the flow rate in the extruder also has to be considered, as well as the material distribution. When combining Equation (2) with the SFL equation, the shear factor SF can be defined, thus allowing to integrate shear and flow rate in one equation [9]

$$\mathrm{SF} = \frac{\dot{\gamma} h D_s^2}{\dot{V}} \tag{3}$$

Here, the shear conditions in the process can be extracted from calculations or numerical simulations. Additionally, if Equation (2) holds, the SF is inversely proportional to SFL.

While SF allows for similar shear conditions, it does not consider the residence time of the material in the extruder or locally within the kneading zones. Therefore, the specific mechanical energy input (SEI), defined by Equation (4), provides an interesting scale-up parameter, which rather reflects the integral stress held by the material during processing [8, 16].

$$\mathrm{SEI} = \frac{P}{\dot{m}} = \frac{t \eta \dot{\gamma}^2}{\rho} \tag{4}$$

The SEI represents the ratio of the mechanical energy applied by the screw to the mass flow rate $\dot{m}$, similar to ε. Here, the mechanical energy can be expressed using the drive power which locally corresponds to the volume-specific internal stress or viscous dissipation, $P_{\mathrm{diss}}/V = \eta \dot{\gamma}^2$, described in terms of the viscosity η and the shear rate $\dot{\gamma}$ [15, 16]. The SEI also integrates the residence time t, making it more versatile than SF. However, the shear rate in the extruder is still not clearly defined in the literature, especially for partially filled extruders [15]. Due to the complex material flow conditions and geometry, it is difficult to describe it with a single value, for instance, Equation (2) can be used to calculate the shear rate at a given channel depth, but fails to describe the entire geometry. Therefore, process simulations make it possible to identify zones of high and low shear rates and accordingly quantify the amount of stress. Additionally, expressing the shear rate as a frequency distribution provides a more accurate representation of how often a given shear rate occurs within the device.

2.2 | Process Simulation

In order to examine the resulting flow profiles during production, a simulation is required since no suitable analytics are available. Using simulations also makes it possible to obtain information about the resulting strain of the material in the extruder, which can be used to precisely determine the SF and SEI, not relying on Equation (2).

Material flowing through the extruder experiences different strain conditions depending on both the process parameters and the screw geometry [14]. In addition, the screw size has a significant effect on the resulting flow profiles due to the changes in flow capacity. If the screw geometry is held constant, the increase in size leads to an increase in flow capacity of the screws.

In this work, the Smoothed-Particle-Hydrodynamics (SPH) method was used to perform flow simulation of the extruder kneading sections for the investigated extruder scales. SPH is a mesh-free simulation method which allows the calculation of fluid flows based on the description of the interaction between mass points also called SPH-particles by solving the Lagrangian Navier Stokes equation for mass and momentum conservation [17]. The viability of the simulation setup for the extruder application for battery slurries has been discussed in our previous works [14, 18]. Please refer to these works for a detailed description of the simulation setup.

Similarly to our previous study, a weakly compressible approach was used to conduct the simulations. This approach is necessary for coupling the mass and momentum equations [17]. In addition, we further improve the accuracy of the simulation by integrating a modified dynamic boundary condition (mDBC) for a

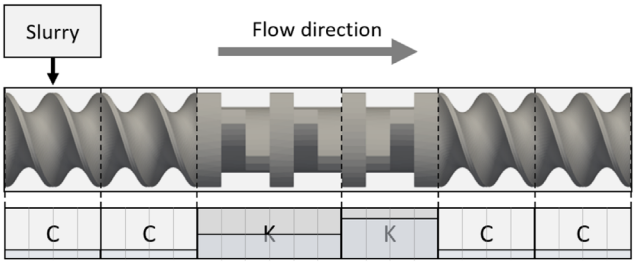

FIGURE 1 | Diagram of the simulation domain and setup, including an inlet baffle for dosing the particle-based fluid (anode slurry) into the first zone, and an outlet condition where particles leaving the screw section are simply removed from the domain. Illustration of the segmentation of the screw section used for post-processing.

better description of the fluid–wall interaction. While the Dynamic Boundary Condition (DBC) is a standard method in SPH applications, due to its straightforward implementation, it often leads to spurious boundary effects that affect the accuracy of the simulations. mDBC provides a more precise estimation of boundary forces, reducing pressure discontinuities at the fluid-solid interfaces, thus increasing the accuracy of the simulations [17]. This was essential for computing the free volume flow in the simulations more efficiently, thus reducing errors in the calculation of the filling level across the screw configuration.

As for the resolution of the simulations, the SPH particle size was adjusted according to the geometry of the different scales, while still allowing enough time steps to reach steady state. For the laboratory and the pilot extruders, a SPH particle size of $d_p = 0.2$mm was used, while for the larger extruder $d_p = 0.25$ mm was used, since a larger extruder requires more particles to be filled and therefore more computational resources. The calculations were performed using the open-source software DualSPHysics [17].

Figure 1 illustrates the setup of the simulation. As shown in the diagram, the simulation focused primarily on the kneading section (K) of the evaluated screw configurations. The slurry was fed into the domain at the first conveyor element (C) via an inlet baffle. To reduce computational effort, particles leaving the domain on the outlet were simply removed.

Material parameters were set constant to 1 Pas for the viscosity and 1500 kgm^{-3} for the slurry density, analogous to our previous work [14]. Moreover, all simulations were performed under identical parameter settings to those used in the experiments in order to recreate equivalent material flow conditions.

3 | Results

3.1 | Analysis of Material Strain and Flow Behavior

An experimental evaluation of the production conditions inside the extruder is usually not possible due to the close build of the process. Nevertheless, the effects can be indirectly measured through the product changes. For this reason, simulations of the process have been used as a calculation method to evaluate

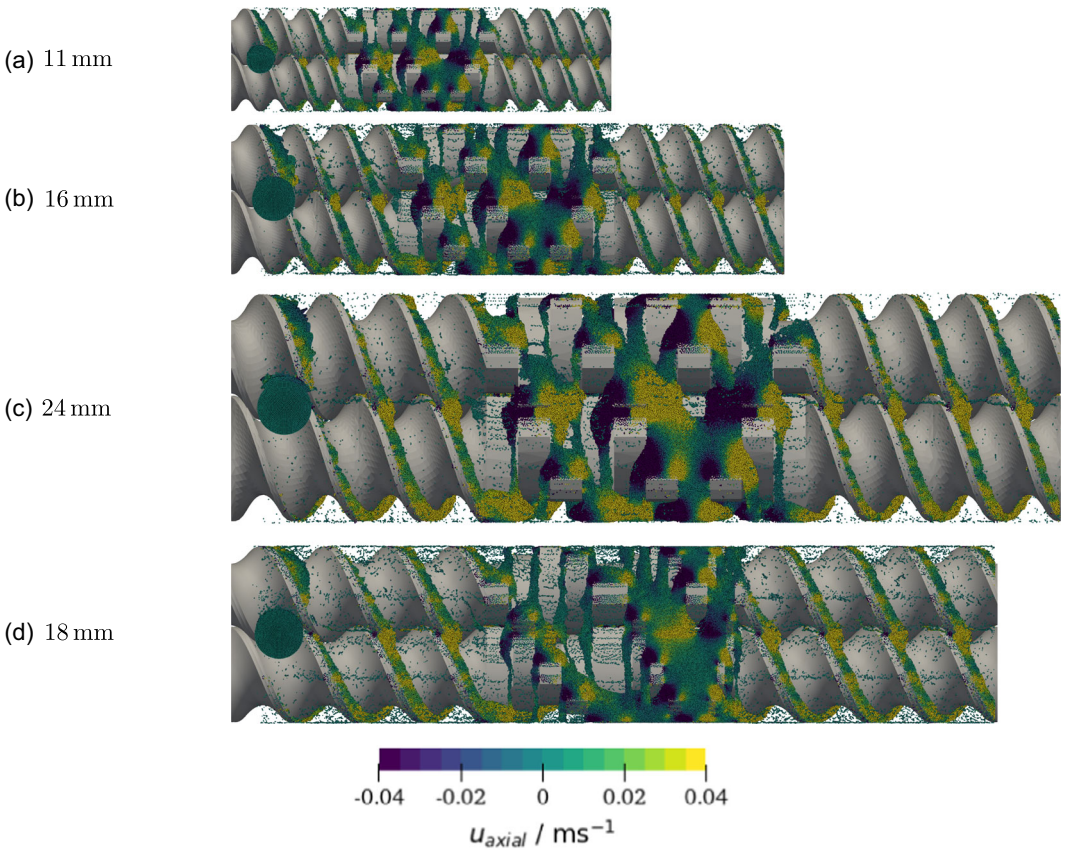

FIGURE 2 | Snap-shots of the simulated flow distribution in the kneading section for equivalent screws (a–c) and an alternative screw (d). Corresponding to a SFL number of around 0.022 for the evaluated screw sizes (11, 16, 18, and 24 mm) at a screw speed of 300 rpm.

the material flow behavior in the different extruder scales prior to experimental analysis to assess the feasibility of the investigated scaling approach. This allowed the comparison of material distribution across the kneading sections by calculating the resulting fill levels and material strains for the different scales.

The material flow behavior is expected to be similar for comparable values of the specific feed load in the extruder. Therefore, a volumetric scale is evaluated as the primary scaling rule. Figure 2 illustrates an example of flow patter in the simulated co-rotating screw sections obtain for the evaluated scales. This been at the equivalent processing conditions based on a same SFL number.

The images are equally scaled so that the screw dimensions on the figure are proportional relative to each other, thus illustrating the relative screw size difference. They show that for the same SFL, similar flow patterns are obtained between the different scales, especially for the geometric equivalent screws (Figure 2a–c). In addition, the alternative screw exhibits a comparable degree of material retention and is also qualitatively similar to the reference screw (TSE-11 mm). In general, a smooth distribution in the conveyors, as well as slurry accumulation in the kneading zone is observed throughout all designs, as expected.

3.1.1 | Local Fill Level

In order to effectively compare the outcomes of the evaluated process conditions, a quantitative analysis of the local fill levels was conducted using the simulations, as shown in Figure 3. The calculations are based on the average amount of particles flowing through each extruder section in 1 second (20 frames) of the simulation in steady state. For better comparison, the kneading sections were discretized based on the width of the kneading discs, i.e., the number of particles every 2.75 mm for the TSE-11 extruder, 4.00 mm for the TSE-16 and for the TSE-18 extruders and 6.00 mm for the TSE-24 extruder. In addition, this discretization was also applied to the conveyors, where it provides a 4-point sampling at each conveyor element, being consistent for all evaluated scales due to a length to diameter (L/D) ratio of 1 for the implemented geometric equivalent extruders. A representation of the resulting discretization can be seen in the Figure 1. In case of the alternative extruder (TSE-18), the applied discretization results in a 6-point sampling at each conveyor element, since the (L/D) ratio is slightly higher.

To obtain the corresponding fill level, the number of particles in each section (Δl) was related to the maximum theoretical number of particles (p) that fit into each geometry at the corresponding resolution (d_p). These were 9147 p mm^{-1} for the TSE-11, 19 728 p mm^{-1} for the TSE-16, 22 356 p mm^{-1} for the TSE-24, and finally 24 112 p mm^{-1} for the TSE-18 extruder. Each value correspond to the number of particles in a fully filled kneading section as generated in the preprocessing step and therefore represent a perfectly ordered state. This theoretical state sets a limit on the number of particles relative to the size of the screw, which allows for comparison of the screw. However, this limit cannot be reached in practice.

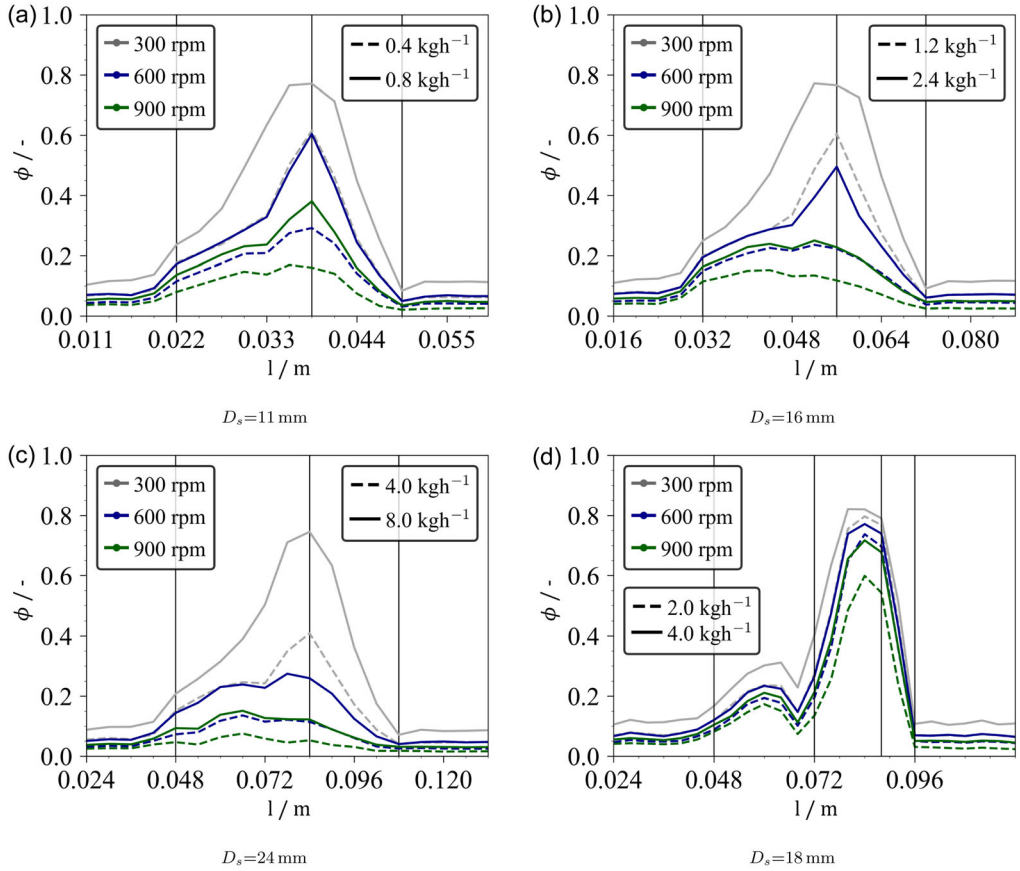

FIGURE 3 | Effects of the extruder screw speed and feed rate on the local fill level ϕ of the kneading zone in extruders with 11 (a) 16 (b) 24 (c) and 18 mm (d) screw diameter gained from simulations. Where (a–c) are geometric equivalent and (d) features an alternative screw configuration. The fill level is plotted along the length l of the screw in the flow direction.

Figure 3 reveals that both higher flow rates and lower screw speeds result in higher fill levels. This is consistent across all investigated scales. Moreover, the resulting profiles manifest a material accumulation just before the backward kneading block, a behavior that was present at all scales and can be attributed to the higher flow resistance of the backward geometry.

In case of having geometric equivalent screws (Figure 3a–c) an identical SFL number results in similar profiles with slightly different absolute fill levels. While these extruders have a constant length to diameter ratio ($L/D = 1$) for each screw element, the laboratory scale has thinner kneading disks compared to the larger scales, which is likely to induce a higher flow resistance. The simulation suggests that at low screw speeds, i.e., at higher fill levels, the resulting local material retention in the kneading section is more comparable between the scales, while at higher screw speeds, i.e., when the fill level is low, the geometrical effect on the flow resistance is more noticeable.

Similarly, while the implemented kneading design for the TSE-18 extruder is comparable to the arrangement used for the geometric equivalent extruders, it exhibits a different filling profile (Figure 3d). Here, the fill level is less dependent on process variations. One reason for this is that the kneading discs are consistently thinner in the flow direction, which again supports a higher flow resistance.

3.1.2 | Local Shear Rate Distribution

The local fill level has an important impact on particle dispersion applications, since it affects both the material strain and the local residence time [14, 15]. To evaluate the effect of screw size on dispersion, the resulting local material stress for the different scales was calculated from the process simulations. This is done by calculating the material strain based on the velocity gradients in the fluid, analogous to our previous work [14, 18]. Figure 4 shows the obtained frequency distributions $q_0(\dot{\gamma})$ of the shear rate in each extruder scale for the different process parameter combinations.

The distributions describe the range and frequency of shear rate values in the kneading zones after the flow has reached a steady state. They are averaged from 1 s (20 frames) of simulation time. This is done to provide a better description of the entire fluid domain, as due to the complex geometry of the screw, zones of high and low shear are formed, making it difficult to approximate the mean strain condition analytically or by simply applying Equation (2).

In general, an increase in screw speed causes an increase in shear rate for all scales and evaluated flow conditions. This been consistent with the expectations of the analytical model given in Equation (2). Likewise, comparable shear rates are obtained for all extruder scales. However, the maximum shear rate value

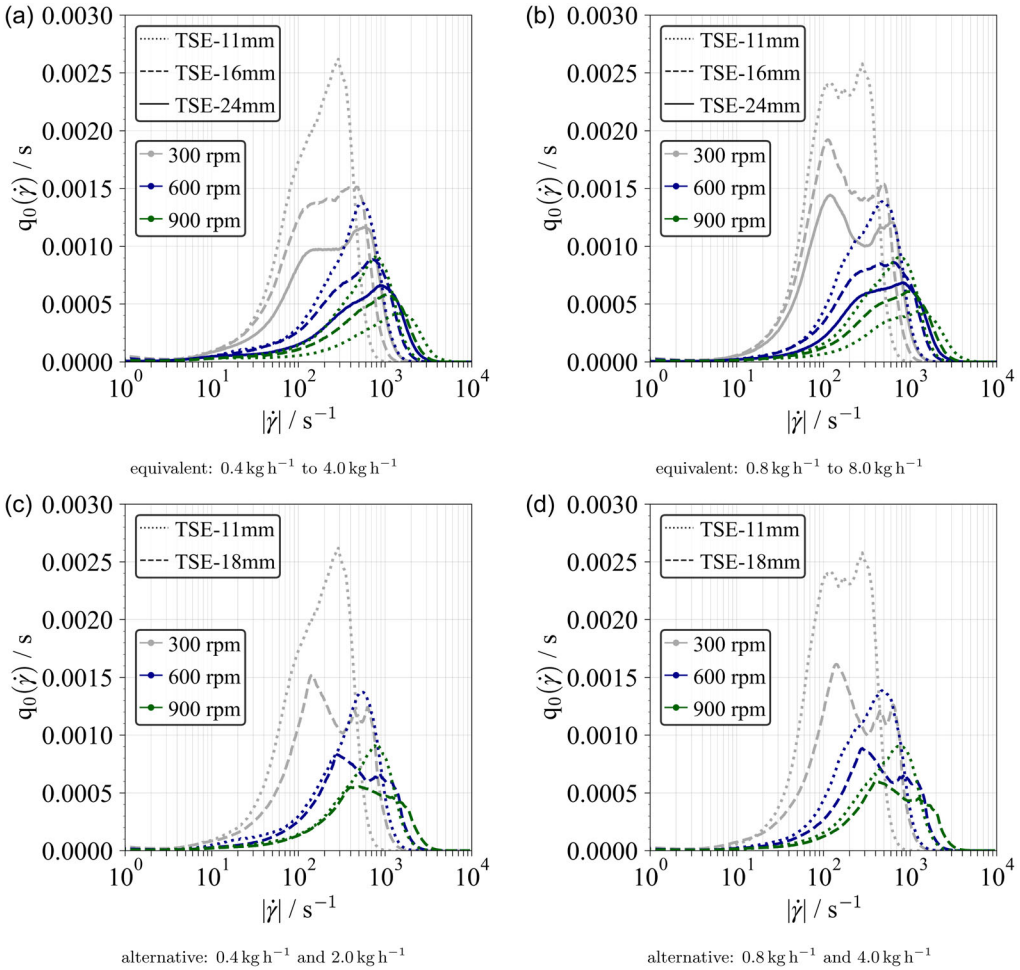

FIGURE 4 | Effects of the screw speed and extruder scale on simulated shear rate frequency distribution ($q_0(\dot{\gamma})$) in the kneading zone for equivalent geometries at respectively lower (a) or higher (b) flow rates and comparison for alternative geometries at respectively lower (c) or higher (d) flow rates.

is greater with a larger screw due to the increase in tip velocity. While the shape of the distribution profiles are comparable, they are shifted towards higher shear rate values as the screw size increases. Note that this data is not directly measurable during the experiments and highlights the benefits of a process simulation. Figure 4a,b illustrate the change in shear rate values for geometric equivalent extruder scales. Here, the shape of the distribution is consistent between scales, reflecting the similarity in flow behavior (fill level) due to the use of an equivalent screw geometry. In contrast, getting the same shear rate behavior from alternative screws is more challenging. Figure 4c,d show a clear difference between the profiles. In case of TSE-18, the peak of the distribution was consistently located towards lower shear rates, reflecting the obtained higher fill levels.

One way to compare the global strain conditions is to calculate the overall stress at each scale using the shear factor (SF) by applying Equation (3). Here, the median value of the shear rates obtained from the simulations is used. Similarly, the average mechanical specific energy input (SEI) is calculated to integrate the mean residence time and reflect the amount and duration of mechanical stress occurring at each setting. Figure 5 shows the resulting SF and SEI values for the different extruders in function of the SFL-number.

For the overall shear rates, a linear relationship between SF and SFL^{-1} is obtained, as expected from Equation (3). This underlines that similar SFL values result in similar shear rates across the evaluated extruder scales, regardless of the geometry.

In comparison, the screw configuration significantly impacts the generated SEI value. While the results indicate that the SEI between different extruder scales is comparable when the SFL number is kept constant, this is only valid for geometric equivalent screws (TSE-11, TSE-16 and TSE-24). Although the SEI values for alternative screw (TSE-18) are similar, they are consistently higher for both feed rates and specially for the lower feed. This can be attributed to the fact that the fill level (see Figure 3) in the TSE-18 was consistently higher than in the other setups; subsequently inducing an increase in residence time, which led to greater SEI values.

On this basis, the simulations suggested that screw geometry significantly affects process conditions and must be considered when transferring production between different scales. Moreover, using the same geometric ratios facilitates flow similarity, which is expected to yield similar product qualities given equivalent process conditions. Likewise, achieving the same process conditions with alternative screw configurations is more challenging and requires a deeper understanding of the process, thus making simulations key to assist the transfer.

3.2 | Scale-Up Effects on Product Quality

Among the main product quality parameters to control in the production of battery slurry are the slurry rheology and its homogeneity or dispersion [1]. Each of these factors directly affects the processability and later the quality of the cells, thus having a great impact on overall cell performance.

3.2.1 | Rheology

The flow characteristic of the slurry has an important effect on the downstream production steps and must therefore remain unaffected when the process is scaled up. Figure 6 shows the measured viscosity profiles of the samples as a function of shear rate.

The profiles show a shear thinning behavior for all samples, which is typical for this type of formulation. The processing range of interest for coating is around 1 Pas [19, 20]. This viscosity range is achieved for shear rates above 100 s^{-1} providing a wide processing bandwidth for coating applications. Moreover, the paste composition was consistent between the different scales. As a result, comparable viscosity behavior was achieved for all samples, resulting in similar flow properties of the slurries regardless of process conditions or extruder size. Small differences between the samples are apparent, specially for shear rates under 100 s^{-1}, however they lie within the expected experimental error.

Nevertheless, the differences in the dosing equipment required for each scale may be responsible for slight discrepancies that affect the dispersion of the binders. Material dosing on the

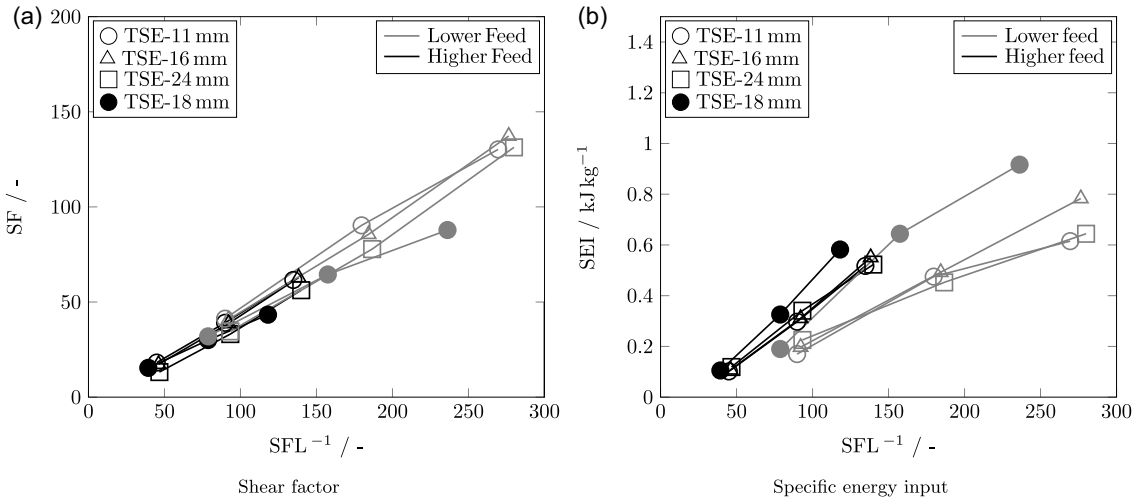

FIGURE 5 | Effects of the process parameters on the simulated average shear factor (a) and specific energy input (b) values in the kneading zone as a function of the inverse value of the specific feed load (SFL^{-1}) for the evaluated extruder scales.

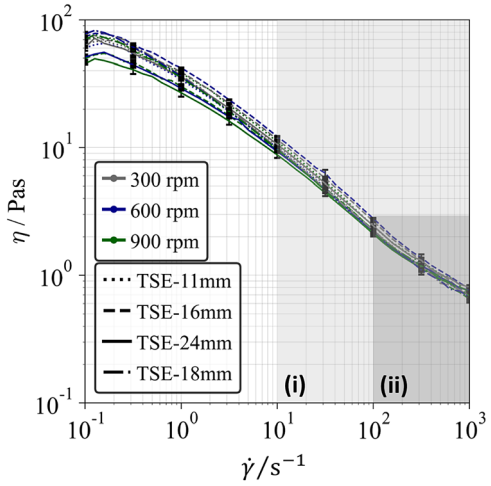

FIGURE 6 | Comparison of the measured shear rate dependency of viscosity of the produced anode slurries at different screw speeds and production scale (screw sizes). Region (i) illustrates the ruling range of shear rates in the process derived from the simulations. Meanwhile, region (ii) highlights the relevant viscosity range at the obtained median shear rates for the evaluated process setups.

smaller scales was more sensitive to feeding fluctuations due to the relatively low flow rates. However, given the shear rates experienced during production and the resulting variations in viscosity, the results suggest that there is no significant alteration to the rheology of the slurry for the evaluated process conditions or formulation, as highlighted in region (i). Furthermore, as shown in region (ii), using a viscosity of 1 Pas for the simulations adequately represents the material behavior for the evaluated process setups.

3.2.2 | Dispersion

3.2.2.1 | **Geometric Screws.** The resulting particle size of carbon black (CB) as a conductive additive is crucial for the resulting microstructure and final battery performance, making it an important quality parameter to preserve during scale-up.

In order to compare the effects of different process conditions on CB dispersion efficiency, particle size distributions of the slurries after extrusion were measured for the evaluated extruder scales. Starting from the 11 mm laboratory scale extruder (TSE-11), it was possible to transfer production to different sizes using the same screw configuration due to the consistent geometric ratios (L/D) of the screw elements. Figure 7 shows the measured extinction-weighted particle size distributions of the slurries produced using the different geometric equivalent screw sizes (11, 16 and 24 mm).

Considering the particle size distribution of graphite and its high concentration of above 90 wt.% in the slurry formulation, the detection of particles with an equivalent diameter greater than one ($x^* > 1\,\mu m$) can be attributed primarily to graphite and some large agglomerates. Similarly, particles with an equivalent diameter of less than one ($x^* < 1\,\mu m$) are considered fines and are attributed primarily to carbon black aggregates and small agglomerates. In addition, previous studies have shown that the detected changes within the evaluated process range can be attributed to changes in the carbon black agglomerate sizes [14].

The distributions reveal a greater amount of fines in the samples with increasing screw speed. This implies that an increase in screw speed promotes the breakage of larger agglomerates, which correlates with the increased shear stress, as discussed in section 3.1. However, this is more pronounced at lower feed rates, a behavior that is present on all evaluated scales. Most importantly, the obtained distributions for the different extruder scales did not show significant differences at equivalent process parameters. This indicates that scale-up of flow rates based on SFL provides comparable dispersion quality, for geometric equivalent screw sizes.

In order to quantitatively compare the degree of dispersion for the investigated settings and scales, the dispersion index (DI_{CB}) of the fines (CB), was calculated from the measured particle size distributions. Similar to the definition introduced by Weber et al. [12], the DI is defined by

$$DI_{CB} = Q(x_{CB})\frac{x_{CB}}{x_{50,CB}} \tag{5}$$

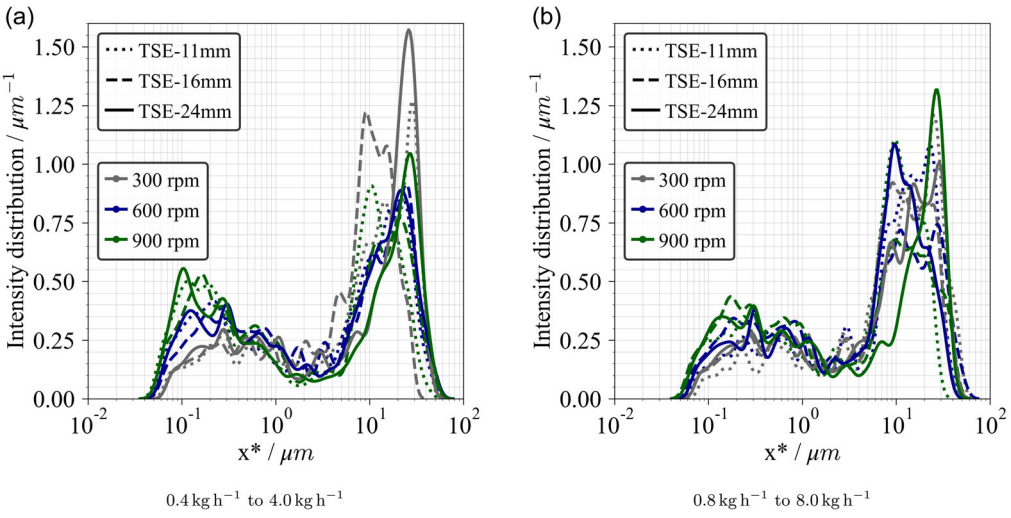

FIGURE 7 | Comparison of the resulting particle size distribution of the produced anode slurries at different screw speeds and sizes for low (a) and high (b) feed rates. Screw configurations feature identical geometry ratios ($L/D = 1$).

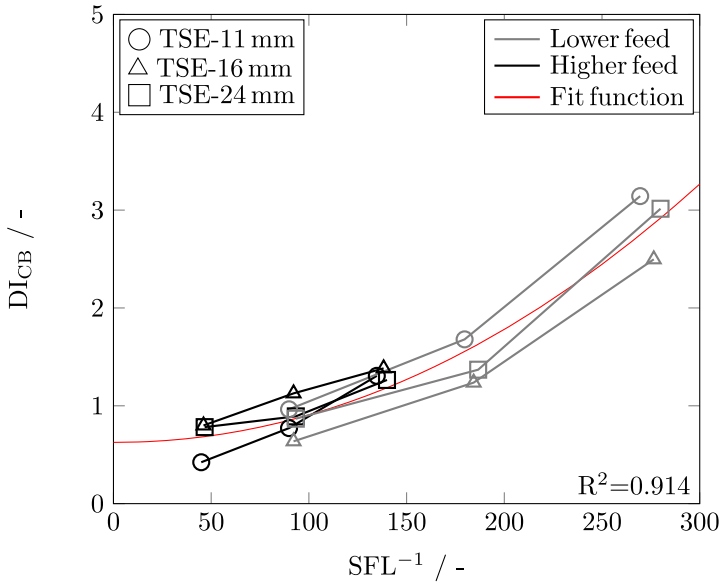

FIGURE 8 | Effect of the screw scale on dispersion index of CB (DI_{CB}) for geometric equivalent screw. Experimental data described by fit function: $DI_{CB} = 2.362 \cdot 10^{-5} (SFL^{-1})^{2.038} + 0.626$.

and describes the amount of fines in the samples $Q(x_{CB})$ times the fraction cut-off x_{CB} divided by the median particle size within the fine fraction. Thus, a higher DI_{CB} value indicates both the presence of a high amount of fines and a high proportion of particles with reduced diameters. For the produced anodes slurries, particles with a diameter smaller than 1 µm have been considered to be fines, i.e., $x_{CB} = 1$ µm. Figure 8 shows the obtained DI_{CB} values in relation to the applied SFL values for the different scales.

In the considered process parameter range, the dispersion index DI_{CB} is consistently higher as SFL^{-1} increases. Likewise, the range of dispersion appears to be depended on the feed rate, i.e., a lower feed rate allows for higher dispersion degrees, this been valid for all evaluated extruder scales and has been found to be analogous to the increase in strain (see Figure 5a). Based on the obtained data, a scale-up with a constant SFL number seems to be sufficient to achieve similar DI_{CB} for geometric equivalent screw geometries. Moreover, considering all data points, an exponential increase in DI_{CB} is apparent. The empirical relationship has been modeled using the power-law, resulting in

$$DI_{CB} = 2.362 \cdot 10^{-5} (SFL^{-1})^{2.038} + 0.626 \quad (6)$$

which describes the obtained data reasonably well ($R^2 = 0.914$). This is remarkable, as Equation (6) describes data from different extruder scales, mass flow rates and screw speeds in a single equation. Also note that the power law approach is consistent with the breakage kernels regularly employed in population balance modeling [21, 22]. For a more precise relationship, further studies should focus on the parameter range of $SFL^{-1} \approx 225$ and $SFL^{-1} > 300$.

SEM imaging of the electrodes allows for a detailed qualitative evaluation of the local material dispersion and homogeneity of the electrode components after extrusion. Figure 9 shows an overview of selected images of the electrodes corresponding to different process conditions and also provides a detailed view of the electrode microstructure.

The images show a comparison between the resulting particle distribution within the electrodes, for anodes produced at the lowest screw speed and the corresponding high mass flow rate (low stress condition) and the highest screw speed and the corresponding lower mass flow rate (high stress condition). The presence of two particle fractions can be seen in the samples, where the large smooth particles correspond to graphite and the smaller rough particle groups (agglomerate) correspond to carbon black and binders, also called carbon binder domain (CBD) [23]. No visible breakage of the graphite fraction was observed for the used formulation in the investigated process parameter ranges. However, considering the CBD, at low screw speeds, only large agglomerates were encountered, whereas at high screw speeds, fewer large agglomerates were observed and a greater number of small fragments were instead obtained. This was found across all investigated scales and supports the increase in the degree of dispersion obtained in the measured particle size distributions.

3.2.2.2 | **Electrode Quality.** The mixing step has a crucial effect on the degree of dispersion and thus on the electrical conductivity of the electrode composites. The objective is to reduce the electrical resistivity of the electrode films in order to enhance the electrical conductivity. To characterize the effect of the different scales on the electrical conductivity in the produced electrode films, measurements of the composite layer resistance were conducted. Figure 10 illustrates the obtained electrode quality, showing the effects of SFL on the resulting electrical resistivity (volume) for the investigated process scales, together with the corresponding electrode thickness and porosity.

The measurements show that the SFL^{-1}, and therefore the applied stress, has a significant effect on the quality of the electrode after coating. It can be observed that at higher SFL^{-1} values the electrical resistivity of the electrodes decreases, thus increasing the conductivity. Electrical resistivity data from all evaluated extruder scales align well, demonstrating that scaling up production rates based on SFL^{-1} and hence SEI results in comparable

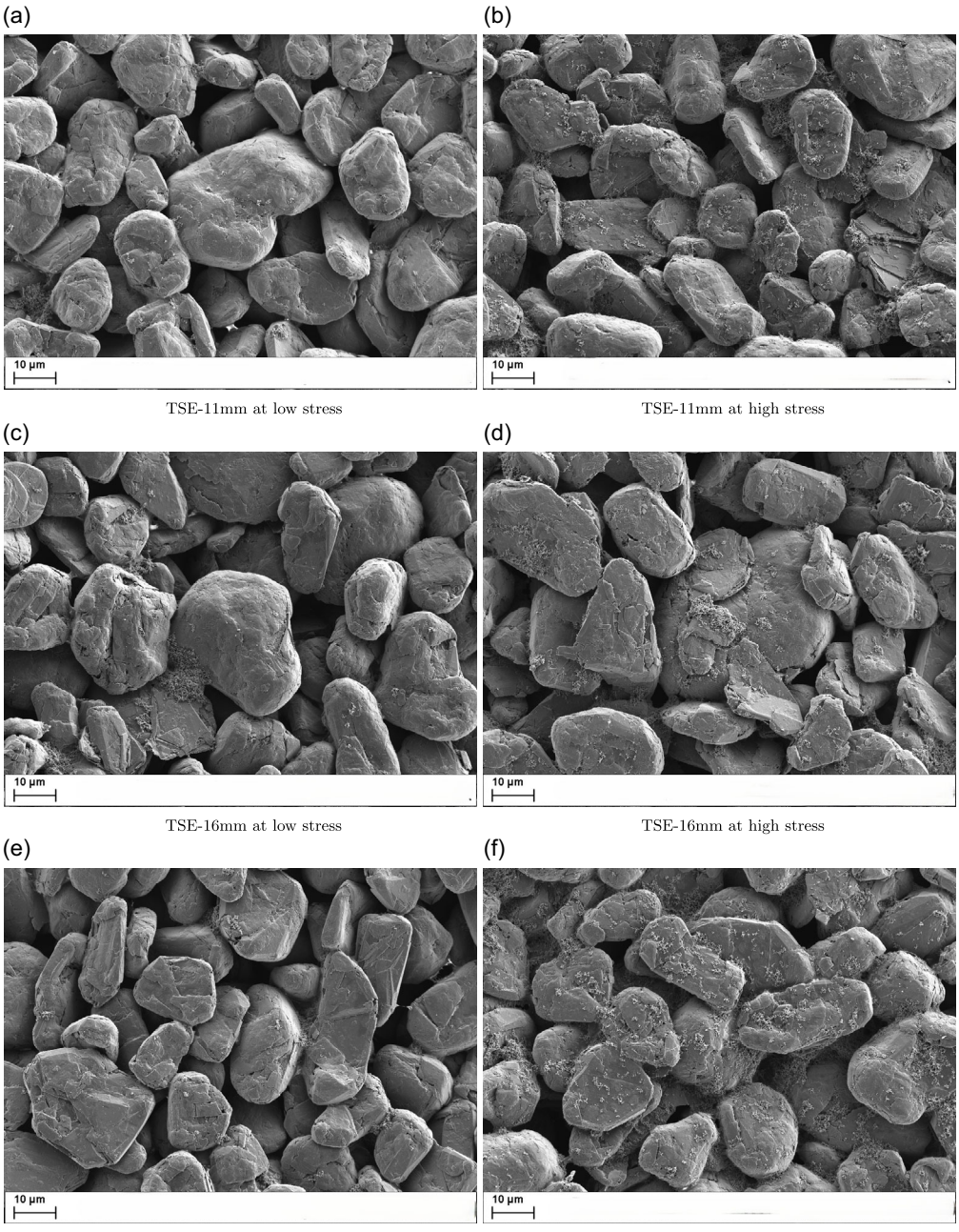

FIGURE 9 | Comparison of the resulting material structure (SEM-images) for electrodes process with different geometric equivalent screw sizes (TSE-11, TSE-16 and TSE-24) at low and high stress conditions. Low stress corresponding to a $SFL^{-1} \approx 45$ and high stress to a $SFL^{-1} \approx 275$.

electrical performance. At $SFL^{-1} \approx 75$ more data points are shown, because the same SFL is achieved by two different combinations of screw speed and mass flow rate. Here, the data points differ significantly. Since no systematic scale-dependence is apparent, these differences are likely caused by experimental errors. As the SFL^{-1} increases and reaches values greater than 100, the electrical resistivity levels out for all scales and the benefits of enhanced dispersion diminish. For SFL^{-1} values below 100 however, higher resistivity values and larger deviations were obtained. Electrode thickness appears to be less consistent at lower SFL^{-1} values, as indicated by an increasing standard deviation. Here, data points from the investigated scales differ significantly, although no clear trend is apparent. It is therefore concluded that the observed differences are most likely due to inconsistencies in the experimental preparation and drying of the electrodes. Similarly but less pronounced, the porosity values at high SFL^{-1} values align well across all scales, while lower SFL^{-1} values result in less consistent electrodes and therefore larger deviations. In addition, it was observed that electrodes processed with lower SFL^{-1} values, i.e., at lower stress conditions, produce a rougher and less homogeneous surface with partially visible carbon black clusters (Supporting Information, Figure S1). In conclusion, all these results indicate that a SFL^{-1} ater than 100 produces electrodes of high quality and consistency. Furthermore, electrode quality can be scaled reliably in this parameter window.

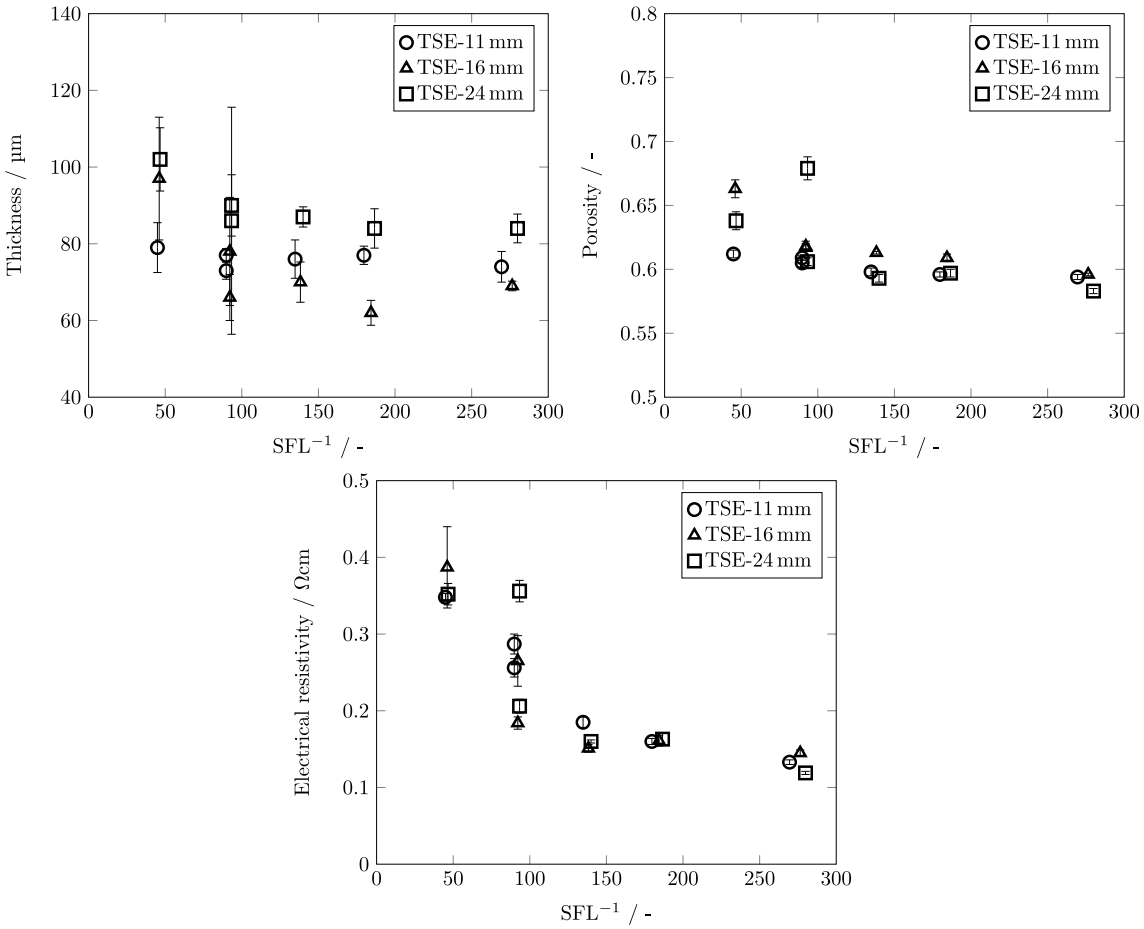

FIGURE 10 | Effect of the induced stress in terms of SFL number on the resulting electrode thickness, porosity and the corresponding composite volume electrical resistivity of the produced electrodes.

3.2.2.3 | **Alternative Screws.** In the case of nongeometric equivalent or alternative screw configurations, the transfer of the degree of dispersion is not as straightforward as for geometric equivalent screws. The different geometries may induce different flow conditions, which affect both the material strain and residence time, as discussed in section 3.1. To overcome this issue, one option would be to modify the target kneading zone, which involves searching for an alternative design closer to the initial configuration so that the integral SEI is again comparable. Alternatively, more kneading section can be added to match the integral SEI of both designs. The latter has been considered in this work using the calculated values of SEI for a single kneading section from the SPH simulations. This way, it was possible to adjust the number of kneaders in the experiment to provide comparable integral SEI values within the processes and thus achieving equivalent dispersions, as shown in Figure 11.

Figure 11a shows that the laboratory scale extruder (TSE-11) with 3 separate kneading zones produces very similar SEI values to the pilot scale extruder (TSE-18) with 2 kneading zones, when SFL is held constant. Consequentially, considering this adaptations, similar DI values were obtained for similar SFL^{-1} numbers (Figure 11b) and again, the DI is increased with increasing SFL^{-1} as expected. Moreover, a clear distinction between high and low feed rate is visible that is traceable to the differences in Figure 11a. For the same SFL number, a higher feed rate induces a slightly higher SEI, resulting in a moderately higher DI, however at lower feed rates higher SFL numbers are possible, allowing higher DI values. This remains valid for all evaluated extruders.

Furthermore, based on Figure 11, SEI was found to be an appropriate scale-up indicator when transferring dispersion quality across different alternative screw designs. By generating a similar average SEI for the different screws, it was possible to recreate again the relationship between DI and SFL even for alternative screws. Similar to the geometric equivalent extruders, this relation has been also modeled using the power-law approach (Equation (7)), which described the data ($R^2 = 0.976$) well and considered both screw designs.

$$\mathrm{DI_{CB}} = 8.261 \cdot 10^{-4} \left(\mathrm{SFL}^{-1}\right)^{1.507} + 0.641. \tag{7}$$

Whereas SEI has been used for scale-up to capture the effects of both strain and residence time in individual kneading zones, as discussed in section 3.1, this method is based on average values of the simulated data and does not take into account the full strain and time distribution in the extruder. Nevertheless, by simply adding the simulated average SEI values according to the number of kneading zones in each screw configuration, it was possible to match the total SEI value for different screws and thus obtain comparable degrees of dispersion in the slurries. A more accurate approach could be achieved by implementing a fully resolved evaluation of the dispersion, such as population balance modeling.

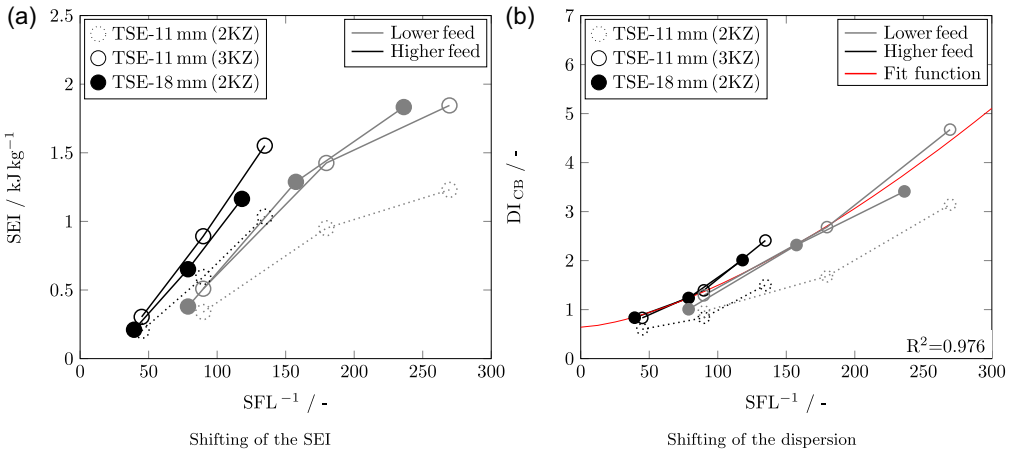

FIGURE 11 | Dependency of the average specific energy input (SEI) for two alternative screws with different amount of kneading zones (KZ) as a function of the specific feed load (SFL) (a) and corresponding impact on the dispersion index (DI_{CB}) of CB in the processed anode slurries (b). Corresponding PSD can be found in Supporting Information, Figure S2. Experimental data described by fit function: $DI_{CB} = 8.261 \cdot 10^{-4} \, (SFL^{-1})^{1.507} + 0.641$.

3.2.2.4 | **Electrode Quality.** In addition, the aim is to transfer dispersion efficiency without compromising the slurry quality, as, e.g., the electrical performance of the electrodes, as shown in Figure 12. Here, electrical resistivity measurements of the produced samples illustrate the effects of adapting the screw configuration with an additional kneading zone, which, as previously discussed, increases the integral SEI, and the direct comparison with a larger nongeometric screw with similar SEI values.

The results show that, similar to the increase in dispersion, the addition of more kneaders also supports a decrease in electrical resistivity as expected. This effect was more pronounced for lower SFL values ($SFL^{-1} < 100$), where in contrast, a less pronounced increase in electrical resistivity was obtained for SFL^{-1} values above 100. Furthermore, when comparing the resulting resistivity profiles obtained for the sample process at similar SEI values, the values obtained are more comparable, which again demonstrates the accurate reproduction of product quality.

4 | Conclusion

This investigation assessed the effect of extruder screw size on dispersion efficiency when scaling up battery slurry production rates. The analysis was divided into scale-up operations using geometric and alternative screw configurations. For this purpose, three different extruder scales with geometric equivalent screws were investigated to demonstrate continuous mixing from laboratory to pilot to production scale. An additional extruder with different geometric ratios was also introduced to further evaluate the effects of screw geometry.

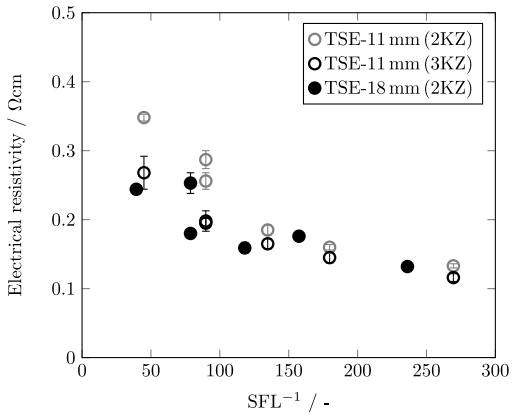

FIGURE 12 | Effect of SFL on resulting electrode volume resistivity for alternative extruders.

By simulating the process prior to the experimental analysis, it was possible to evaluate the resulting flow behavior at different scales, taking into account the increment in production capacity. For the investigated process range, the simulations always showed a partial filling of the kneading section. Moreover, when comparing the resulting filling profiles for screws with the same geometric ratios, it was found that keeping the SFL constant resulted in similar local fill levels across the extruder. This was essential as it affects the local residence time in the extruder. In addition, screw geometry becomes more relevant when comparing the response of the nongeometric screw to process changes. The fill levels were less susceptible to changes caused by process parameters.

Regarding the material strain, for a given screw speed and fill level, a larger screw will induce a slightly higher shear rate due to the increase in tangential velocity. First, the stress factor (SF) has been evaluated to ensure comparable shear rates in the different process, revealing that for all evaluated process conditions and scales at the same SFL value, similar average stress conditions are applied to the slurries. For the geometric equivalent screws, even though the screws have the same L/D ratio, a wider kneading disk induces less flow resistance, which results in a reduced filling, which also results in a slightly shorter residence time. Therefore, it appears that even though the average shear is higher, the reduced residence time compensates for the dispersing effect. Resulting also in a consistent SEI value between the different scales. In contrast, for an scale-up operation between screws with different geometric ratios, SEI evaluation resulted to be key to ensure the transfer and enhancement of the dispersion efficiency.

The measurement of the changes in the particle size distribution demonstrated that the dispersion efficiency can be transferred to larger scales by keeping the SFL value constant if an equivalent SEI value is applied. This was qualitatively confirmed by SEM

analysis. The results have shown that scale-up based on SFL is feasible for geometric equivalent screws, while for alternative screws, SFL can be used if the integral SEI induced by both screws is similar. This can be done, for example, by adjusting the number of kneaders in the screw to subsequently match the integral SEI. Finally, this allowed the modeling of the relationship between the dispersion and the process parameters in terms of SFL^{-1} for both geometric and nongeometric screw scales. A power law approach was found to describe the obtained data reasonably well in both cases with a $R^2 > 0.9$.

Regarding product quality after scale-up, the rheological properties of the slurries were consistent and showed no large variation between all evaluated process conditions, providing similar flow behavior for coating in all setups. Similarly, the effect of SFL^{-1} on electrode quality was shown to be similar on all scales: For the evaluated process conditions, a SFL^{-1} lower than 100 was identified to partially provide rough surfaces and visible carbon black clusters, which are characteristics for low quality electrode, where as in contrast for higher SFL^{-1} values uniform film thickness and porosity values were obtained, as well as lower electrical resistivity values. Adjusting the screw design to achieve higher integral SEI values allowed for higher dispersion and therefore lower resistivity at lower SFL^{-1} values.

This work demonstrates how the continuous production rates of battery slurries can be scaled up without compromising critical product parameters. In the scope of a growing demand for batteries and rapidly evolving new material systems, this is crucial information for industry. It further highlights the benefits of process simulations in this area: SPH simulations reveal nonmeasurable data such as shear rate distributions, which in turn are essential for making informed scale-up decisions. This even allows for a scale-up between alternative screws, i.e., screws from different manufacturers, a process that usually relies on experience and heuristic rules. In essence, this study provides information and methods that have an impact in making large-scale electrification a reality.

5 | Experimental Section

5.1 | Evaluated Twin-Screw Extruder Scales

To evaluate the scaling behavior of the continuous battery slurry production, two scenarios have been considered. The first approach was to ensure geometric similarity of the devices for proper comparison of the results. For this purpose, three different extruder sizes of the same manufacturer, Thermo Fisher Scientific (Germany), were used: one on laboratory scale, one on pilot scale, and one on production scale. This allows the use of similar screw configurations with the same geometric aspect ratios ($L/D = 1$). For laboratory scale, a Thermo Scientific Energy 11 (TSE-11) extruder was used. The pilot scale extruder corresponds to the Thermo Scientific Process 16 (TSE-16) and the production scale extruder to the TSE 24 MC (TSE-24). The extruders have a nominal screw diameter of 11, 16, and 24 mm respectively. In addition, the ZSK-18 extruder from Coperion (Germany) with a nominal screw diameter of 18 mm was investigated. Its different geometry ratios allow the assessment of scale-up to nongeometric equivalent or alternative screws. Figure 13 provides an overview of the geometric dimensions of each investigated machine.

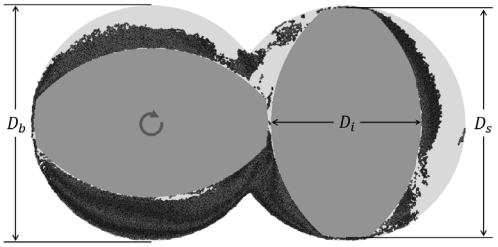

Scale	D_s	D_i	D_b	L_T
	mm	mm	mm	mm
TSE-11	10.70	6.20	11.00	440.00
TSE-16	15.60	9.10	16.00	640.00
TSE-24	23.60	13.70	24.00	960.00
TSE-18	17.90	11.62	18.30	720.00

FIGURE 13 | Overview of the evaluated extruder geometry parameter: screw outer diameter (D_s), screw inner diameter (D_i), barrel diameter (D_b), and screw total length (L_T).

The screw configuration in all scales combines an arrangement of conveyors and two separate kneading sections. For the geometric equivalent screws, the kneading section consists of kneading disks arranged with an offset angle of 60°. Additionally, in order to obtain a higher local fill level in the kneading section, the last four kneading disks are set in opposite direction of rotation to induce flow retention in the kneading section, thereby causing a higher flow resistance. This arrangement resembles the screw configuration studied in our previous work [14]. Similarly, the kneading zones in the 18 mm extruder, consisted on an arrangement of three standard kneading blocks with offset angle of 45°. In order to maintain a comparable section length, we used a 24 mm in combination with a 16 mm block and a 8 mm backward kneading block at its end to also induce flow retention in the kneading section.

5.2 | Experimental Procedure

The mixing step in battery production is meant to homogenize the battery components and disperse the conductive additive. In the case of wet mixing, a solvent is used to facilitate dispersion and produce a slurry. For the production of anode slurries, graphite is usually used as an active material (AM), and its conductivity is enhanced by adding a conductive additive such as carbon black (CB). Binders and additives are used to ensure stability of the electrode microstructure during production and in the cell. In water-based anodes, carboxymethylcellulose (CMC) and styrene-butadiene rubber (SBR) are commonly used [1, 19, 20]. The anodes in this study are water-based with a solid content of 43%, the used formulation for the solid fraction was introduced in our previous work [14] and consisted of 93%wt graphite, 1.4%wt CB, 1.87%wt CMC and 3.73%wt SBR. The graphite used in this study was Mechano-Cap 1P1 (HC Carbon Gmbh) with an average particle size of 20–24 µm. The conductive additive used was Super C65 conductive carbon black (Nanografi Nano Technology), and the binders were carboxymethylcellulose sodium salt (Carl Roth) with a degree of substitution of 0.75–0.85 and styrene-butadiene rubber (Nanografi Nano Technology) [14].

The anode slurry components were separated into the wet and dry dosing ports and continuously fed into the process. In the

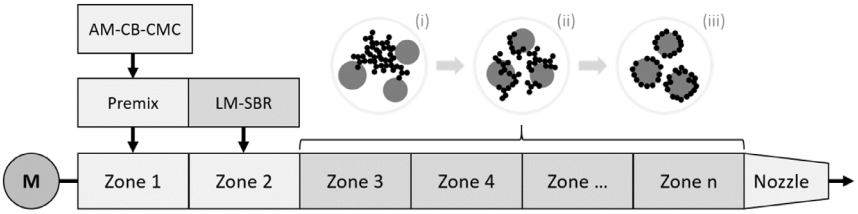

FIGURE 14 | Schematic diagram of the extruder setup including material dosing ports for a dry premix of graphite (AM), carbon black (CB) and carboxymethylcellulose (CMC), as well as for liquid fractions of distilled water (LM) and styrene-butadiene rubber (SBR). Graphical representation of the expected changes to the material microstructure during production: initial state (i), CB breakage (ii), and AM surface saturation (iii) [24].

first extruder zone, dry components, consisting of graphite, carbon black, and CMC, were dosed by mass using gravimetric feeders. Subsequently, a diluted SBR-water solution was introduced into the process at the third extruder zone using a peristaltic pump. Figure 14 provides a schematic diagram of the described process setup.

The anode slurries were processed at the same screw speeds of 300, 600 and 900 rpm and according to the scale, the mass flow rates were adjusted. The flow rate was scaled based on the SFL number, as discussed in section 2.1. For practical purposes, the increase in feeding rates was calculated using factors of 3, 5 and 10, respectively. Starting from the laboratory scale (TSE-11), the flow rates were chosen to be 0.4 and 0.8 kgh^{-1}, accordingly for the pilot scales (TSE-16) and (TSE-18), and for the production scale extruder (TSE-24) the flow rates are 1.2 and 2.4 kgh^{-1}, 2.0 and 4.0 kgh^{-1} and 4.0 and 8.0 kgh^{-1}, respectively. Moreover, the experiments were run from the lowest screw speed, followed by switching between the evaluated mass flow rates before increasing the screw speed to avoid a rapid increase in energy input, which could potentially distort the samples.

5.2.1 | Quality Control

Two key quality parameters to assess are the rheology of the slurries, which determines processability and the particle size distribution which represents the microstructure in the slurries. These parameters should remain constant, when production is scaled up. Therefore, to trace quality alterations, anode slurry samples (30 mL) were taken during extrusion for all process conditions, after a minimum of 5 min following each process change to ensure steady flow. In order to trace the effects on the product quality the particle size distributions of all samples were measured using a LUMiSizer (LUM GmbH). The working principle of the device is based on measuring variations in light intensity during sedimentation of particles in a centrifugal field. As a result, time-dependent sedimentation profiles are obtained, and particle sizes can be derived. Due to the measurement method, the particle size distributions obtained are light-intensity weighted. To avoid hindered settling due to high particle concentration, a dilution of 1:100 anode slurry in water was found to be suitable. The measurement script consisted of a two-step centrifugation procedure. The first step applied a rotational speed of 500 rpm for 5 min. Here, sedimentation of graphite and also large carbon black agglomerates was observed based on the time-dependent light transmission profiles, which converged after the first centrifugation step. Afterwards, the centrifugal force was increased to 4000 rpm for 2 h for detection of smaller agglomerates and aggregates (fine particles) in the probes, at the end of which, a clear liquid phase was obtained [14].

In order to evaluate the effect of process conditions and scale on the slurry flow characteristics, the rheology of the produced samples was measured using a plate–plate rheometer from Bohlin Instruments GmbH (Typ CVO HR NF/C-VOR) with a gap size of 1 mm and a plate diameter of 20 mm.

To further compare the scale-up effects on slurry performance, electrode quality after coating of the slurries was measured using scanning electron microscopy (SEM) and electrical resistivity as key indicators of integrity preservation. For this purpose, the anode slurries were coated onto a copper foil with a coating gap of 180 µm on an automatic film applicator (PG-1818V from Thierry GmbH) and then slowly dried at room temperature to mitigate binder migration effects. The electrical properties were measured using a electrode resistance measurement system (RM2610 from HIOKI E.E.).

List of Symbols

Nomenclature

d_p SPH particle size	mm
DI Dispersion index	–
D_b Barrel diameter	mm
D_i Inner screw diameter	mm
D_s Outer screw diameter	mm
h Gap size	mm
l Axis length (section)	m
L Screw length	mm
M Torque	N m
$\dot{m}$ Mass flowrate	$kg\,s^{-1}$
n Screw speed	rpm
SF Shear factor	–
SEI Spec. mech. energy input	$J\,kg^{-1}$
SFL Specific feed load	–
t Residence time	s
$\dot{V}$ Throughput	$m^3\,s^{-1}$
x Particle diameter	µm
$\dot{\gamma}$ Shear rate	s^{-1}
ϵ Spec. mech. energy consumption	$J\,kg^{-1}$
ϕ Fill level	–
η Viscosity	Pa s
ρ Density	$kg\,m^{-3}$

Author Contributions

Juan Fernando Meza Gonzalez: conceptualization (lead), data curation (lead), formal analysis (lead), investigation (lead), methodology (lead), software (lead), validation (lead), visualization (lead), writing – original draft (lead). **Annika Völp:** conceptualization (supporting), resources (lead), writing – review and editing (supporting). **Hermann Nirschl:** conceptualization (supporting), funding acquisition (lead), project administration (equal), writing – review and editing (supporting). **Frank Rhein:** conceptualization (supporting), project administration (equal), supervision (lead), writing – review and editing (lead).

Acknowledgments

Support from Project Management Jülich [PTJ] within the research cluster InZePro is highly acknowledged. The authors acknowledge support from the state of Baden–Württemberg through bwHPC and the KIT–Publication Fund of the Karlsruhe Institute of Technology. The authors acknowledge the support of Julia Gandert for the measurement of the electrode porosity. Pirmin Koch is acknowledged for assistance with SEM measurements. Kristóf Kalocsai is acknowledged for assistance with the extrusion process. Thermo Fisher Scientific is acknowledged for allowing the use of part of the machines.

Open Access funding enabled and organized by Projekt DEAL.

Funding

This study was supported by Bundesministerium für Bildung und Forschung (03XP0369A).

Conflicts of Interest

The authors declare no conflicts of interest.

Data Availability Statement

The data that support the findings of this study are available from the corresponding author upon reasonable request.

References

1. J. Li, J. Fleetwood, W. B. Hawley, and W. Kays, "From Materials to Cell: State-of-the-Art and Prospective Technologies for Lithium-Ion Battery Electrode Processing," *Chemical Reviews* 122, no. 1 (2022): 903-956.

2. D. Grießl, A. Adam, K. Huber, and A. Kwade, "Effect of the Slurry Mixing Process on the Structural Properties of the Anode and the Resulting Fast-Charging Performance of the Lithium-Ion Battery Cell," *Journal of the Electrochemical Society* 169, no. 2 (2022): 020531.

3. K. Arslan, K. B. Dermenci, J. Van Mierlo, and M. Berecibar, "Current and Future Trends in Lithium-Ion Battery Electrode Production Machinery: A Comprehensive Review," *Applied Energy* 402 (2026): 126968, https://doi.org/10.1016/j.apenergy.2025.126968.

4. H. Patil, S. K. Vemula, S. Narala, et al., "Hot-Melt Extrusion: From Theory to Application in Pharmaceutical Formulation—Where Are We Now?," *AAPS PharmSciTech* 25, no. 2 (2024): 37.

5. J. Wesholowski, K. Hoppe, K. Nickel, C. Muehlenfeld, and M. Thommes, "Scale-Up of Pharmaceutical Hot-Melt-Extrusion: Process Optimization and Transfer," *European Journal of Pharmaceutics and Biopharmaceutics* 142 (2019): 396.

6. J. Matić, A. Witschnigg, M. Zagler, S. Eder, and J. Khinast, "A Novel in Silico Scale-up Approach for Hot Melt Extrusion Processes," *Chemical Engineering Science* 204 (2019): 257.

7. A. Nastaj and K. Wilczyński, "Optimization and Scale-Up for Polymer Extrusion," *Polymers* 13, no. 10 (2021): 1547.

8. E. E. Agur, "Extruder Scale-Up in a Corotating Twin-Screw Extrusion Compounding Process," *Advances in Polymer Technology* 6, no. 2 (1986): 225.

9. K. Kohlgrueber and M. Smith, *Co-Rotating Twin-Screw Extruders: Applications*, 1st ed. (Hanser Publications, 2020).

10. B. Dryer, G. Fukuda, J. Webb, et al., "Comparison of Scale-up Methods for Dispersive Mixing in Twin-screw Extruders," *Polymer Engineering & Science* 57, no. 3 (2017): 354.

11. H. Potente, K. Kretschmer, and J. Flecke, "A Physical-mathematical Model for the Dispersion Process in Continuous Mixers," *Polymer Engineering & Science* 42, no. 1 (2002): 19-32.

12. M. Weber, J. K. Mayer, and A. Kwade, "The Carbon Black Dispersion Index DI_{CB} : A Novel Approach Describing the Dispersion Progress of Carbon Black Containing Battery Slurries," *Energy Technology* 11, no. 5 (2023): 2201299.

13. M. Weber, J. Gerstenberg, and A. Kwade, "Impact of CB Dispersion on the Performance of Lithium-Ion Battery Cathodes," *Journal of Energy Storage* 99 (2024): 113244.

14. J. F. Meza Gonzalez, H. Nirschl, and F. Rhein, "Continuous Anode Slurry Production in Twin-Screw Extruders: Effects of the Process Setup on the Dispersion," *Batteries* 10, no. 5 (2024): 145.

15. K. Kohlgrueber and M. Smith, *Co-Rotating Twin-Screw Extruders: Fundamentals*, 1st ed. (Hanser Publications, 2019).

16. M. Grundler, Optimierung der thermischen Leitfähigkeit hochgefüllter Graphit-Polymer-Compounds zur Wärmeableitung (Ph.D. Thesis, University of Duisburg-Essen, 2021), https://doi.org/10.17185/duepublico/74586.

17. J. M. Domínguez, G. Fourtakas, C. Altomare, et al., "DualSPHysics: From Fluid Dynamics to Multiphysics Problems," *Computational Particle Mechanics* 9, no. 5 (2022): 867-895.

18. J. F. Meza Gonzalez and H. Nirschl, "Numerical Investigation of the Local Shear Rate in a Twin-Screw Extruder for the Continuous Processing of Li-Ion Battery Electrode Slurries," *Energy Technology* 11, no. 6 (2023): 2201517.

19. J. Kumberg, W. Bauer, J. Schmatz, et al., "Reduced Drying Time of Anodes for Lithium-Ion Batteries through Simultaneous Multilayer Coating," *Energy Technology* 9, no. 10 (2021): 2100367.

20. F. Jeschull, D. Brandell, M. Wohlfahrt-Mehrens, and M. Memm, "Water-Soluble Binders for Lithium-Ion Battery Graphite Electrodes: Slurry Rheology, Coating Adhesion, and Electrochemical Performance," *Energy Technology* 5, no. 11 (2017): 2108.

21. R. I. Jeldres, P. D. Fawell, and B. J. Florio, "Population Balance Modelling to Describe the Particle Aggregation Process: A Review," *Powder Technology* 326 (2018): 190.

22. J. Pandya and L. Spielman, "Floc Breakage in Agitated Suspensions: Theory and Data Processing Strategy," *Journal of Colloid and Interface Science* 90, no. 2 (1982): 517.

23. J. Entwistle, R. Ge, K. Pardikar, R. Smith, and D. Cumming, "Carbon Binder Domain Networks and Electrical Conductivity in Lithium-Ion Battery Electrodes: A Critical Review," *Renewable and Sustainable Energy Reviews* 166 (2022): 112624.

24. V. Wenzel, H. Nirschl, and D. Nötzel, "Challenges in Lithium-Ion-Battery Slurry Preparation and Potential of Modifying Electrode Structures by Different Mixing Processes," *Energy Technology* 3, no. 7 (2015): 692-698.

Supporting Information

Additional supporting information can be found online in the Supporting Information section. **Supporting Fig. S1:** Comparison of the surface quality of the electrodes produced at the lowest and highest evaluated process stress conditions in different extruder scales. **Supporting Fig. S2:**

Comparison of the resulting particle size distribution of the produced anode slurries at different screw speeds and sizes for low (a) and high (b) feed rates. Screw configurations feature different geometry ratios.